


Dynamics of complex systems in Cauchy cavities

Ruitao Wu  and Aristide Dogariu*

CREOL, The College of Optics & Photonics, University of Central Florida, Orlando, Florida 32816, USA

 (Received 29 November 2021; revised 15 March 2022; accepted 6 April 2022; published 27 April 2022)

We demonstrate a generalized invariance property: that the ratio between the intrinsic dynamics of complex media and the perceived timescale of scattered intensity fluctuations depends only on macroscopic properties and not on the detailed circumstances of geometry-dependent light-matter interaction. We show that the necessary conditions can be established in a diffusive Cauchy cavity where the relation between these two timescales can be controlled at will. This approach provides the flexible means to study the intrinsic dynamics of systems with arbitrary geometry and in various conditions of interaction.

DOI: [10.1103/PhysRevA.105.043523](https://doi.org/10.1103/PhysRevA.105.043523)

I. INTRODUCTION

Fluctuations of scattered intensity encode the time-varying properties of complex media [1]. To extract the information, inverse problems must rely on accurate description of the process of light-matter interaction. For instance, the widely used dynamic light-scattering procedure was designed for the strict limit of deterministic single scattering [2]. When the interaction enters a regime of multiple scattering, the dynamic inverse problem can be approached using a diffusing wave spectroscopy (DWS) methodology [3,4]. In this case, however, the constraint is that one requires additional information about the path length s of light through the medium. What is needed, practically, is the probability density function $P(s)$ of optical path lengths inside the medium, a quantity that intimately depends on the experimental circumstances [5]. Because analytical solutions for $P(s)$ exist only for certain special cases, the approach has a limited applicability [5–9].

Certain invariance properties exist for extreme conditions of interaction between monochromatic light and finite-size inhomogeneous media [10]. For instance, according to Cauchy's mean-chord theorem [11,12], in the ballistic regime, the mean path length $\langle s \rangle = \int_0^\infty P(s)s ds$ of the scattered light is solely determined by the volume and the effective surface of the medium. A similar conclusion can be reached for a diffusive regime: $\langle s \rangle$ depends on the size of the medium but not on the microscopic characteristics of the interaction process [10,13,14]. Importantly, these conclusions are valid only when both the illumination and detection are homogeneous and isotropic across the surface [10,13].

Here we will generalize this essential property to dynamic regimes of interaction. We will also show how this fundamental invariance permits extracting the timescale of medium's dynamics irrespective of the specific experimental geometry and the scattering regime. In other words, we will demonstrate that time-varying properties can be obtained without detailed knowledge of $P(s)$.

II. THEORY

Let us consider light scattering from a complex system of identical particles, which diffuse thermally with a Stokes-Einstein diffusion coefficient D . A straightforward extension can account for biased diffusion as well as the many-body collective effects [15,16]. For an incident field with wave number k_0 , the fluctuations of light have a microscopic characteristic time $\tau_0 = 1/(2Dk_0^2)$. The goal of a generic experiment is to retrieve τ_0 from the measured field-field correlation function $g(\tau) = |\langle E(0)E^*(\tau) \rangle| / |\langle E(0) \rangle|^2$, which is characterized by a measured correlation time τ_m . The challenge is that these two timescales are not necessarily the same. Their ratio τ_0/τ_m depends on the strength of light-matter interaction as quantified by the reduced scattering coefficient μ'_s that defines different scattering regimes [17], as suggested in Fig. 1.

When μ'_s is much smaller than the size of the medium, the perceived characteristic time becomes $\tau_m = 1/(Dq^2)$, where $q = 2k_0 \sin(\theta/2)$ is the corresponding transfer wave vector as defined by the specific experimental geometry. In this single-scattering regime, the macroscopic size and shape of the medium are irrelevant and one can easily find that $\tau_0/\tau_m = 2 \sin^2(\theta/2)$. This regime is denoted by the black dashed line in Fig. 1, where τ_0/τ_m is simply a geometry-dependent constant [2].

With increasing μ'_s , we enter a regime of stronger light-matter coupling where the relation between τ_0 and τ_m becomes rather complicated. Experimentally, due to the internal dynamics of the medium, random phases will accumulate at the detector and contribute to the measured field-field correlation [4]. It has been shown that the coupling between the intrinsic dynamics τ_0 and the measured field-field correlation is determined by the distribution of photon path lengths $P(s)$ [5,18]. When $\tau \ll \tau_0$, the measured field-field correlation function turns out to be [5]

$$g(\tau) = \int_0^\infty P(s) \exp\left(-s\mu'_s \frac{\tau}{\tau_0}\right) ds. \quad (1)$$

In general, a series of higher-order moments of $P(s)$ are necessary to describe $g(\tau)$ in an intermediate regime of

*adogariu@creol.ucf.edu

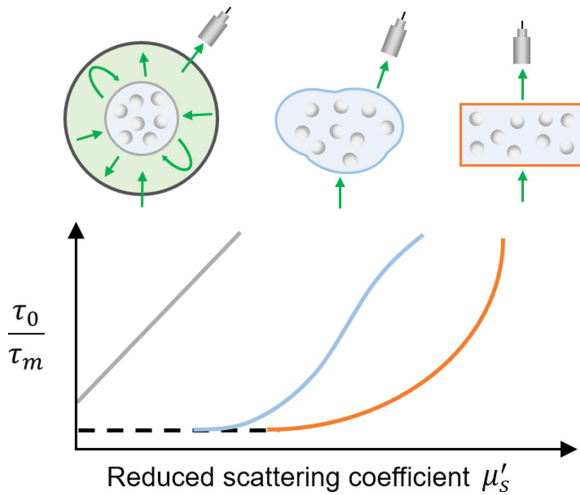


FIG. 1. Log-log representation of ratio between the microscopic τ_0 and perceived τ_m correlation times for different regimes of light-matter interaction. In the single-scattering limit, τ_0/τ_m is purely a geometry-dependent constant (black dotted line). When the coupling increases, τ_0/τ_m depends strongly on μ'_s , the measurement geometry, and also the macroscopic properties of the medium, as suggested by the middle blue line. Analytical solutions may be found only for limiting situations such as, for example, transmission through a two-dimensional diffusive and infinitely extended slab (right orange line). The left gray line depicts the ideal circumstances of the Cauchy cavity discussed in this paper (see text for details).

interaction as shown in Fig. 2. However, in the limit $\tau \ll \tau_0/(\mu'_s \langle s \rangle)$, the measured correlation time τ_m depends only on the first moment $\langle s \rangle$ of $P(s)$ (see Appendix A), and, consequently, $\tau_0/\tau_m = \mu'_s \langle s \rangle$. This means that, in the limit of very short times, the outcome of the dynamic measurement is

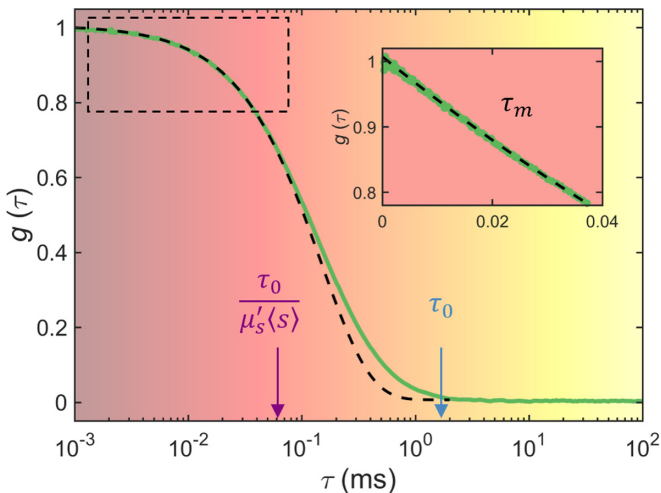


FIG. 2. Measured field-field correlation function $g(\tau)$ (green line) in the strong-scattering regime of light-matter interaction depends on both τ_0 and the path-length distribution $P(s)$. In the short-time limit, $\tau \ll \tau_0/(\mu'_s \langle s \rangle)$, the perceived timescale τ_m is found from the single-exponential decay of $g(\tau)$ (black dashed line and also the inset). Thus, τ_0 can be extracted using solely the mean $\langle s \rangle$ without having to know the explicit form of $P(s)$ or its higher-order moments.

solely determined by $\langle s \rangle$ and knowledge of the entire $P(s)$ is not necessary.

In general, both $\langle s \rangle$ and $P(s)$ depend on (i) the microscopic characteristics of scattering events, (ii) the macroscopic properties of medium, and (iii) the measurement configuration. This is why analytical solutions can only be found in certain limiting situations such as, for instance, diffusive transmission through a slab [19], which is denoted by the right orange line in Fig. 1. We note that, even in this case, the solution accuracy strongly depends on the applicability of the diffusion approximation as well as the detailed boundary conditions [20–22]. For other geometries as suggested by the middle blue line in Fig. 1, one must appeal to numerical approaches [23]. Alternatively, one could directly measure $P(s)$ by time-of-flight or broadband interferometric techniques [24,25], but this process will still be geometry dependent. These are the reasons why it remains a challenge to determine the ratio τ_0/τ_m and, therefore, to extract the *microscopic* dynamic characteristic time τ_0 in a general manner irrespective of the *macroscopic* properties of the medium.

There are two possible ways to overcome this situation. One can, for instance, try to enforce the single-scattering regime, but this is often difficult to ensure in practice [26]. The opposite approach would be to transfer the interaction into a fully developed multiple-scattering regime in a manner in which $\langle s \rangle$ can be easily determined. So far, this second alternative has not been examined for a finite amount of samples. In the following we will show how to achieve it by appealing to the so-called generalized Cauchy invariance property [13,14].

When radiation interacts diffusively with a bounded medium, the mean path-length light is simply determined by the overall volume V and surface area Σ of the medium through which it propagates [13]:

$$\langle s \rangle = 4 \frac{V}{\Sigma}. \quad (2)$$

The caveat is that this assumes that the illumination and detection is performed uniformly across the medium [27]. Practically, light must be injected and detected homogeneously with all possible wave vectors.

This apparently impossible situation can be realized by embedding the dynamic medium into a disordered photonic cavity in which light is injected through a single-mode fiber. We will call this a Cauchy cavity (schematically depicted in Fig. 1) because it homogenizes the field across the surface of the dynamic medium under test ensuring therefore that the conditions for the Cauchy invariance are satisfied. In addition, the highly reflective surface of such cavity increases dramatically the averaged residence time of photons within the medium, which, in turn, guarantees a diffusive regime of light-matter interaction. Under these conditions, one finds that

$$\frac{\tau_0}{\tau_m} \frac{1}{\mu'_s} = 4 \frac{V}{\Sigma}, \quad (3)$$

which constitutes a generalization of the Cauchy invariant property to dynamic media. The meaning of Eq. (3) is that, for light diffusing in a Cauchy cavity, the product between the averaged number of dynamic scattering events and the strength of light-matter interaction depends only on the macroscopic properties of the dynamic medium.

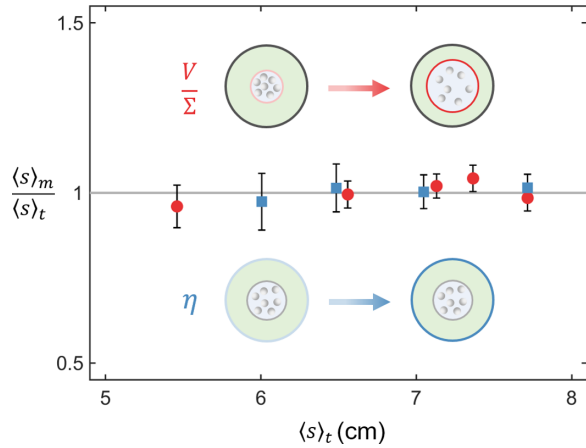


FIG. 3. Comparison between measured mean path $\langle s \rangle_m$ and the prediction $\langle s \rangle_t$ from Eq. (4) for dynamic media with similar microscopic but different macroscopic properties (V/Σ : red circle, η : blue square). The error bars are evaluated by propagating the fitting errors from measurements of $g(\tau)$ and indicate 95% statistical confidence.

In practice, the volume and surface are effective macroscopic parameters associated with both the physical dimensions of the dynamic medium and the optical properties of the Cauchy cavity. As we detail in Appendix B, the refractive index contrast n at the physical boundary of the dynamic medium and the possible cavity losses η can be accounted for in a practical formulation for the averaged mean path:

$$\langle s \rangle = 4 \frac{V_{\text{eff}}}{\Sigma_{\text{eff}}} = 4 \frac{V n^2}{\Sigma \eta}. \quad (4)$$

Here, n^2 is a refractive-index correction for the radiative transfer equation solution in a medium subjected to the aforementioned isotropic and homogeneous radiation condition [27], while η extends the properties of the diffusive walks in the bounded domains [28].

III. RESULTS AND DISCUSSION

The dynamic functionality of the Cauchy cavity is demonstrated on colloidal media consisting of monodisperse polystyrene particles. Measurements were taken inside a disordered cavity (diffusive integrating sphere) in which coherent light (532 nm) was injected using a single mode fiber. A separate nonpolarizing single-mode fiber collects the light from inside the cavity and redirects it into two single-photon detectors. A standard cross-correlation technique is used to measure the temporal correlation function $g(\tau)$. A detailed description of the experiment is included in Appendix C.

We will first validate Eq. (4) using dynamic media with different macroscopic properties. The media are suspensions of particles with diameter of 1 μm and volume concentration of 0.1%, which ensures that both the intrinsic timescale τ_0 and the strength of light-matter interaction μ'_s are the same for all samples. The results summarized in Fig. 3 correspond to situations where the size of the dynamic medium changes (red) or where the effective cavity surface is modified (blue) by opening additional ports. The experimental value of the mean-free path $\langle s \rangle_m = \tau_0 / (\mu'_s \tau_m)$ is compared to $\langle s \rangle_t$ esti-

ated from Eq. (4) by adjusting either the geometry quantity V/Σ (red circle) or the boundary conditions by tuning η (blue square). The η is tuned by opening the number of ports of the integrating sphere. As can be seen, the modified Cauchy invariance of Eq. (4) describes very well the experimental data across the entire range of macroscopic parameters.

There are two more notable observations. First, the experiment summarized in Fig. 3 provides direct experimental demonstration of the invariance property of optical paths in diffusive systems with adjustable reflective and absorbing boundaries [28]. Second, it demonstrates that one can tune the macroscopic parameters of the systems (V , Σ , and η) in a deterministic way to ensure a strong coupling between light and matter, $\mu'_s(s) \gg 1$, and therefore create the circumstances where this invariance property can be applied. This means that in a Cauchy cavity one can actually achieve a regime of diffusive interaction for arbitrarily complex media.

The second series of tests involved weakly scattering media consisting of polystyrene particles with 1- μm diameter and volume fractions ρ ranging from $2.2 \times 10^{-4}\%$ to 1%. The samples were placed in identical transparent containers and four different experiments were performed for each of them both inside and outside the Cauchy cavity. The experimental geometries and a summary of results are shown in Fig. 4. The conditions of this measurement are such that $V/\Sigma = 2.3$ mm, $n = 1.33$, and $\eta \approx 0.21$ as described in Appendix C. The intrinsic dynamic time τ_0 is calculated from the Stokes-Einstein equation while μ'_s is obtained from the corresponding Mie calculations [29].

As can be seen in Fig. 4(a), the results of the measurements performed outside the cavity depend significantly on the experimental conditions as expected. In practice, this complicates significantly the procedure of inferring τ_0 for a given μ'_s as suggested already in Fig. 1. On the other hand, for measurements taken inside the Cauchy cavity, a clear -1 slope can be seen in the log-log representation for samples with $\rho > 0.01\%$. Moreover, this happens irrespective of the angle at which the measurement is performed. It is evident that, in this case, the mean path of diffusive photons $\langle s \rangle$ does not depend neither on the microscopic scattering process nor on the specific measurement geometry. We also note the higher absolute values of the effective path length, which confirm that inside the cavity light is considerably more diffusive. For samples with $\rho \ll 0.01\%$, the measurements are deviated from the prediction of Eq. (4), due to the finite photon lifetime within the system.

In Fig. 4(b), we plot the average path length for samples with $\rho > 0.01\%$. One can clearly see that $\langle s \rangle$ remains invariant with respect to the concentration of particles for measurements taken inside the cavity, while it varies considerably for the other experimental conditions. Most importantly, the value of $\langle s \rangle$ corresponding to measurements inside the Cauchy cavity are very well described by the prediction in Eq. (4). We also note the accuracy of the index contrast and cavity-loss corrections described in Eq. (4) and indicated by the gray dashed line in Fig. 2(b).

Finally, we will show how this Cauchy cavity approach can be used to retrieve the characteristic time of arbitrarily complex dynamic media. To this end, we adjust the dynamic

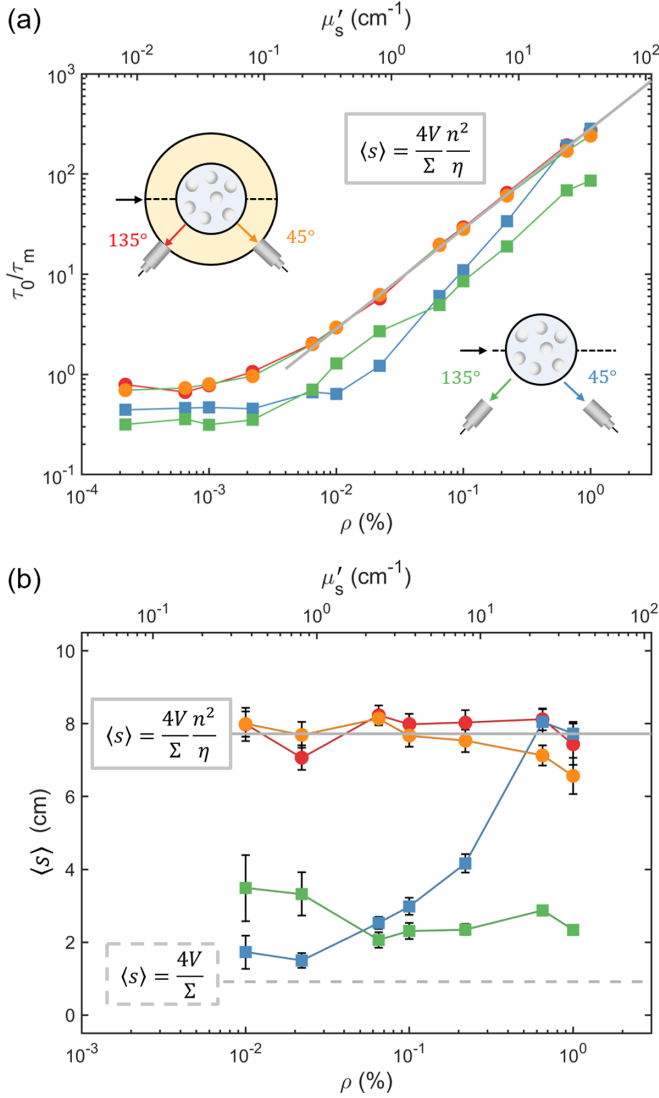


FIG. 4. (a) Ratio τ_0/τ_m for different experimental geometries: inside the disordered cavity at 45° (orange circle, top) and 135° (red circle, top), outside the cavity at 45° (blue square, bottom) and 135° (green square, bottom), respectively. Samples are $1\text{-}\mu\text{m}$ -diameter polystyrene spheres in diameter, of different concentration ρ (x axis at the bottom) and μ'_s (x axis at top). The gray line indicates the prediction of $\tau_0/\tau_m = \mu'_s \langle s \rangle$ with $\langle s \rangle$ from Eq. (4). (b) Values of mean optical path length of light. Note the strong dependence of outside cavity measurements (blue and green squares) on both experimental geometry and scattering regime. On the other hand, the values of $\langle s \rangle$ measured inside the cavity (red and orange circles) are independent of concentration and are very well described by Eq. (4). The error bars indicate 95% statistical confidence.

time by tuning the particle size while keeping the same μ'_s of all the samples. The measured diffusion coefficient D_m is compared with the value D_0 predicted by the Stokes-Einstein equation and the results are summarized in Fig. 5. The relatively larger error for the $3\text{-}\mu\text{m}$ -diameter particles is due to significant hydrodynamic interactions in this case [30]. As evident, the expected internal dynamics is recovered very well in all cases even without knowing the actual $P(s)$.

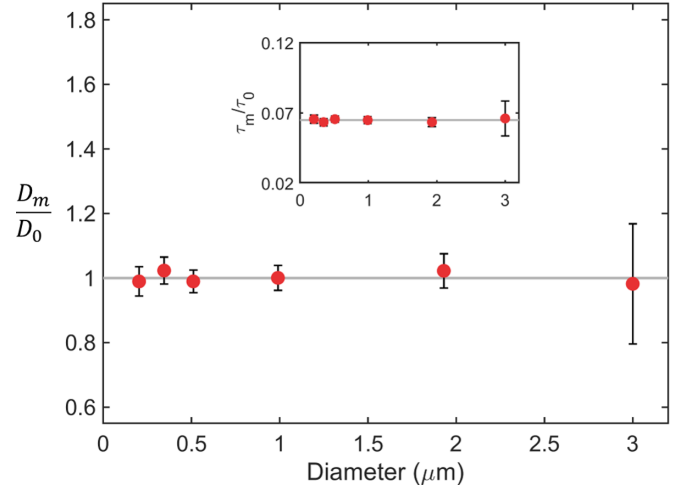


FIG. 5. Diffusion coefficient of colloidal media measured inside the Cauchy cavity reproduces very well the predictions of Stokes-Einstein relation. Inset: the ratio between the measured τ_m and the intrinsic time τ_0 for the media examined. The error bars indicate 95% statistical confidence.

IV. CONCLUSION

We demonstrated a general framework for recovering the characteristic timescale for dynamic media with arbitrarily complex light-matter coupling. The approach relies on the fact that, in strong light-scattering regime, the short-time limit of the dynamics relates only to the first-order moment $\langle s \rangle$ of the optical path length of light. In general, $\langle s \rangle$ is difficult to obtain either analytically or experimentally, but we have established that a general invariance property for diffusive light can be invoked to mitigate this limitation. We experimentally demonstrated that the necessary conditions of strong light-matter interaction are created when measurements are taken inside a disordered cavity with highly reflected boundary conditions, which we called a Cauchy cavity. Besides, we have provided experimental evidence that the Cauchy invariance property for diffusive light can be extended to bounded domains with reflective and absorbing boundaries.

We have also shown that the range of measured characteristic times within the Cauchy cavity can be adjusted at will either geometrically or optically, such that the validity of the diffusive approximation for light propagation is ensured even for weakly scattering media. Moreover, if desired, the approach described here can also be extended to subdiffusive regimes of light propagation, $\tau_0/(\mu'_s \langle s \rangle) < \tau \ll \tau_0$, in the zero to intermediate Knudsen number limit [31]. A short-path statistic argument can be used to generalize Eq. (4) as $\langle s^n \rangle \approx \alpha_n (\mu'_s)^{n-1}$, where α_n is a purely geometric quantity [31,32]. A corresponding measured correlation time can then be obtained from $g(\tau)$ and used to retrieve τ_0 . Similar approach might also be developed for absorbing random media, where the invariance property breaks [33].

In closing, we would like to discuss several possible applications of the Cauchy cavity. As a proof of concept, we have confirmed that accurate characteristics of thermal dynamics can be retrieved irrespective of macroscopic properties of the medium or the strength of light scattering. This opens up new

opportunities for studying dynamic processes in situations in which noninvasive testing would otherwise be prohibited.

For example, the interaction of light with biological systems such as cellular systems often falls in intermediate regimes which are neither weakly scattering nor strongly diffusive [34–37]. In these circumstances, measurements within a Cauchy cavity would still benefit from the noninvasiveness provided by elastic scattering of soft radiation to recover the relevant dynamic scales.

In addition, fundamental processes of anomalous diffusion with different origins (hydrodynamics, many-body interactions, long-range influences, etc.), are usually examined at mesoscales where the strength of coupling between the material system and the probing light is difficult to control [16,38,39]. Here too a Cauchy cavity would provide access to a broad range of timescales for systems with comparable macroscopic sizes. Similarly, in practical situations where the internal structure of complex media changes in time [40–43], our approach would permit a continuous observation of their multiscale intrinsic dynamics even if, during this evolution, the optical regime of interaction changes.

Finally, often the dynamics of complex media varies in response to external influences [44,45]. In many situations, this is accompanied by structural modifications that change the overall circumstances in which the matter scatters light [46,47]. Taking advantage of the ability to uniformize the conditions of interaction one could, for instance, explore the properties of active media in response to various stimuli or even examine the strong coupling between complex media and external fields [48,49].

APPENDIX A: CHARACTERISTIC TIME IN THE SHORT-TIME LIMIT

Following the DWS theory, in multiple-scattering regime, the field-field correlation function $g(\tau)$ is given as follows [5]:

$$g(\tau) = \int_0^\infty P(s) \exp\left(-\frac{s}{l^*} \frac{\tau}{\tau_0}\right) ds. \quad (\text{A1})$$

As mentioned before, $P(s)$ is the probability distribution of photon path length, while $\tau_0 = 1/(2k_0^2 D)$ is the time donating the dynamics of a single object. Note that this equation works for the regime where $\tau \ll \tau_0$ [5]. A generic routine to retrieve τ_0 is to perform fitting of $g(\tau)$ within this range using the knowledge of $P(s)$. This means that detailed knowledge of $P(s)$ is necessary.

However, the same goal can also be achieved by using only the short-time limit where $\tau \ll \frac{l^*}{\langle s \rangle} \tau_0$ [14]. In this case, one can actually take the Taylor expansion of the correlation function and obtain

$$\begin{aligned} g(\tau) &\approx \int_0^\infty P(s) \left[1 - \frac{s}{l^*} \frac{\tau}{\tau_0}\right] ds \\ &= \int_0^\infty P(s) ds - \frac{1}{l^*} \frac{\tau}{\tau_0} \int_0^\infty P(s) s ds \\ &= 1 - \frac{1}{l^*} \frac{\tau}{\tau_0} \langle s \rangle \approx \exp\left(-\frac{\langle s \rangle}{l^*} \frac{\tau}{\tau_0}\right). \end{aligned} \quad (\text{A2})$$

Equation (A2) suggests that, in this limit, the field-field correlation function can be approximated by a single expo-

ponential. Its characteristic time is only associated with the first moment of the optical path length $\langle s \rangle$, instead of the detailed $P(s)$. Therefore, one can define the characteristic time τ_m of the $g(\tau)$ at the short-time limit as

$$\tau_m = \frac{l^*}{\langle s \rangle} \tau_0. \quad (\text{A3})$$

APPENDIX B: INVARIANCE PROPERTIES OF DIFFUSIVE LIGHT IN BOUNDED DOMAINS

In this section, we will derive the invariance property for diffusive light in a bounded domain with boundary conditions [Eq. (4)]. This is necessary because the invariance property has been rigorously derived only for diffusive walks in bounded domains and taking into account the boundary condition as well as the subdomain [28,50]. For diffusive light, the boundary conditions with refractive index mismatch have been examined before [14,27]. The goal of this section is to extend the invariance property of diffusive walks to diffusive light in bounded domains and associate it with the temporal measurements inside the Cauchy cavity.

To start with, we consider the diffusion walks in three dimensions inside a bounded complex system of volume V_0 , as depicted in Fig. 6(a). The outer envelope of a bounded system Σ_0 can be considered as the sum of an absorbing component with surface $\Sigma_{0,abs}$ and one reflective with surface $\Sigma_{0,ref}$ (with unity reflectivity) to practically have $\Sigma_0 = \Sigma_{0,abs} + \Sigma_{0,ref}$. As this is a purely diffusive system, any diffusive walk would eventually reach the absorbing portion of the boundary. We assume that the diffusive walks starts only on the surface of the absorbing boundary, with isotropic and uniform intensity. It has been shown that, under such condition, we can obtained

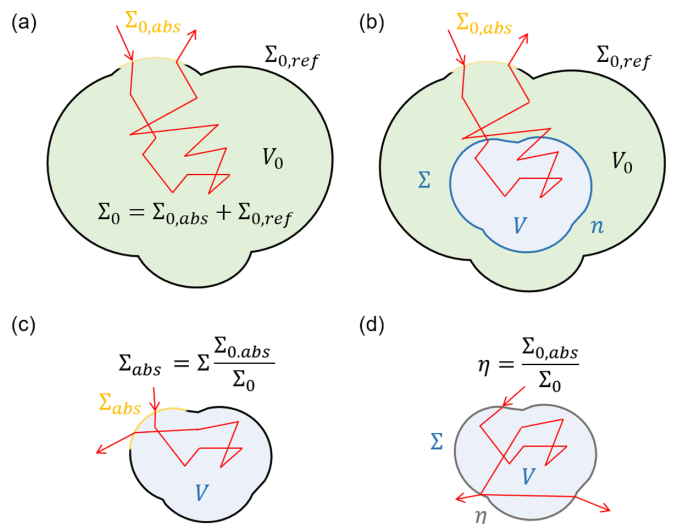


FIG. 6. (a) Diffusive walks in bounded domains, with absorbing $\Sigma_{0,abs}$ and reflective $\Sigma_{0,ref}$ boundaries. (b) Diffusive walks in the subdomain of a bounded system. (c) The equivalent system in (b), but with an absorbing boundary Σ_{abs} and a corresponding reflective boundary. (d) A similar system of (c), but with uniform partial reflective boundary (η represents the loss of the boundary).

the mean-path length of these diffusive walks as [50]

$$\langle s \rangle_{\Sigma_{0,\text{abs}}} = \frac{4V_0}{\Sigma_{0,\text{abs}}}. \quad (\text{B1})$$

Next, we consider a subdomain of volume V inside V_0 , as illustrated in Fig. 6(b). In this case, if we consider the random walks that start and end on the absorbing boundary, we will obtain the mean path length of the diffusive walks inside the subdomain V to be [28]

$$\langle s \rangle_{\Sigma_{0,\text{abs}}} = \frac{4V}{\Sigma_{0,\text{abs}}}. \quad (\text{B2})$$

Now, to extend this conclusion to diffusive light inside a bounded system, a correction regarding the volume must be made to account for the mismatch to the isotropic and homogeneous radiation. This is due to the refractive index mismatch of the layer between the subdomain V and other regime of V_0 , which can be characterized by the refractive index contrast n [14,27]. The n^2 term comes from the correction over the irradiance density between the mismatch layer, which is a consequence of the stationary solution of the radiative transfer equation [27,51]. Thus, we have

$$\langle s \rangle_{\Sigma_{0,\text{abs}}} = \frac{4Vn^2}{\Sigma_{0,\text{abs}}}. \quad (\text{B3})$$

We would like to emphasize again that Eq. (B3) describes the mean path length of photons inside V whose trajectories start and end in the absorbing boundary $\Sigma_{0,\text{abs}}$. However, experimentally only diffusive walks inside the volume V will contribute to the measured temporal correlation function. We can approximate this by decreasing the size of bounded domain until $V \approx V_0$ and $\Sigma \approx \Sigma_0$, as shown in Fig. 6(c). This will lead to

$$\langle s \rangle_{\Sigma_{\text{abs}}} = \frac{4Vn^2}{\Sigma_{\text{abs}}}, \quad (\text{B4})$$

where $\Sigma_{\text{abs}} = \Sigma \times \Sigma_{0,\text{abs}}/\Sigma_0$.

Finally, one can define the loss at the boundary $\eta = \Sigma_{0,\text{abs}}/\Sigma_0$ by assuming that the loss appears uniformly across the surface of the subdomain. This means that instead of applying an absorbing and reflected boundary, it is equivalent to consider a system with boundaries of uniform but nonunity reflectivity ($R = 1 - \eta$). We note that this will not affect the launching conditions for the diffusive random walk. The corresponding physical picture is shown in Fig. 6(d). Note that this can be considered as an ergodic-type generalization of the previous invariance property in bounded domains [28]. Therefore, it is easy to start from Eq. (B4) and obtain the relation for the mean path length of diffusive light in such a system:

$$\langle s \rangle = \frac{4Vn^2}{\Sigma\eta}, \quad (\text{B5})$$

which is Eq. (4).

We note that Eq. (B5) is obtained in three-dimensional disordered media. It can be generalized to other dimensionalities by simply replacing the number 4 with other dimension-

dependent constant η_d [28]:

$$\langle s \rangle = \eta_d \frac{Vn^2}{\Sigma\eta}, \quad (\text{B6})$$

where $\eta_d = \sqrt{\pi}(d-1)\Gamma[(d-1)/2]/\Gamma(d/2)$ and d represents the dimensionality of the system.

APPENDIX C: METHODS

1. Experimental setup

A sketch of our experimental setup is shown in Fig. 7(a). The light source is a green continuous wave laser (Spectra Physics, Excelsior, 532 nm, 100 mW), which is coupled into a single-mode fiber (Thorlabs, P1-460B-FC2) and directed into an integrating sphere (Thorlabs, IS200-4, internal diameter ~ 5 cm, 99% reflectivity), which serves as the disordered cavity. For the detection, we use a fiber coupler (Thorlabs, TN532R5F1) to split the light into two single-photon detectors (PDM, MicroPhoton Devices). A time-correlated single-photon counting correlator card (TimeHarp 260, PicoQuant) is used for measuring the temporal correlation function $g(\tau)$, which has the dynamic range from 10^{-7} to 10^{-1} s. We note that the after-pulsing of such detectors can cause issues when resolving the $g(\tau)$ at very short times, which typically happens around 10^{-5} s. This effect, however, can be mitigated using the cross-correlation scheme of the measured signals from two independent detectors, as shown in Fig. 7(b). The total measurement time for each temporal correlation function is 5 min. There are three main types of losses: the nonunity reflection of the cavity surface, the colloidal absorption, and the absorption of the sample. In all the experiments, the absorption of the diffusive surface ($R = 0.99$) and that of the colloidal suspension are negligible. The loss is primarily due to the absorption of the sample container. The total loss factor of the system was measured to be $\eta = 0.21$ by comparing an empty sample with reflective port plug, each during a total measurement duration of 1 h. As shown in Fig. 3, additional loss factor can be induced by opening more ports on the integrating sphere. Each such port will add approximately 0.015 loss by calculating the ratio between its area and the internal surface of the integrating sphere.

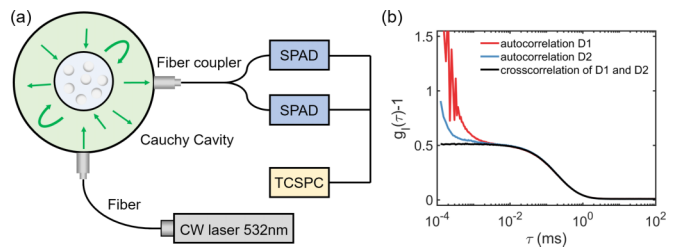


FIG. 7. (a) Sketch of the experimental setup. (b). An example of after-pulsing at short-time limit of $g(\tau)$ from performing autocorrelation of the measured signal from two detectors (red and blue curve for two separate detectors). The cross correlation of signals from these two detectors eliminates the spurious after-pulsing effects (black curve, bottom).

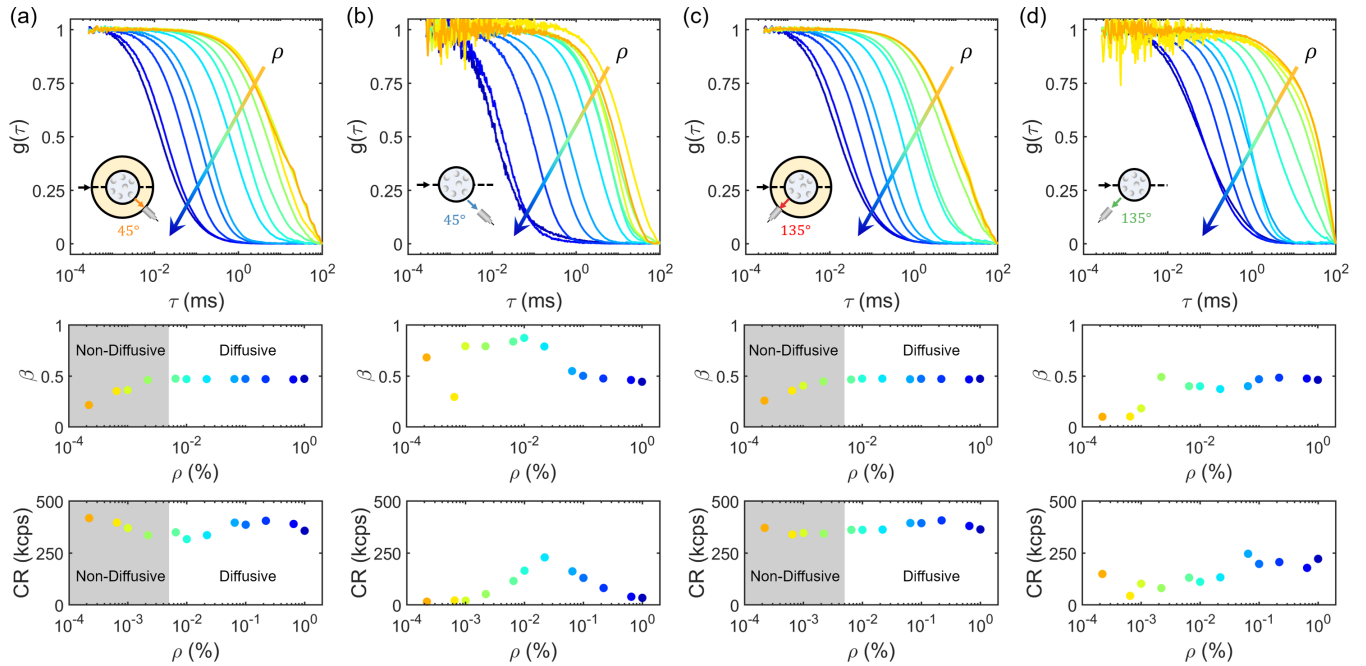


FIG. 8. Comparison of measurements taken at different geometries over different range of concentrations ρ : inside (a) and outside (b) the Cauchy cavity at 45° ; inside (c) and outside (d) the Cauchy cavity at 135° . First column: the normalized field-field correlation function $g(\tau)$. Arrow indicates the increasing of concentrations ρ . Second column: β retrieved from the Siegert relation. Third column: count rates measured by both detectors.

2. Data processing

For each measured $g(\tau)$, the following process is used to retrieve the characteristic time of the dynamics τ_c . First, we normalize each $g(\tau)$ from 0 to 1. Next, we select only $g(\tau) \in [0.8, 1]$ to perform a single-exponential fitting, in which the decay rate of the exponential function is τ_m . This ensures the condition $\tau \ll \tau_0 I^*/\langle s \rangle$ as discussed in the main text and Appendix A.

APPENDIX D: EXPERIMENTAL DATA

1. Comparison of measurements taken inside and outside the Cauchy cavity

We prepared dynamical systems using polystyrene particles of $1\text{-}\mu\text{m}$ -diameter in water, with different volume concentrations, ranging from $2.2 \times 10^{-4}\%$ to 1% . The sample container is identical transparent cylindrical bottles (dimensions: ~ 9 mm in diameter, ~ 15 mm in height). We note that the size of the samples must be much smaller than the diameter of the integrating sphere to ensure the homogeneous illumination condition. The sample container is placed at the center of the sphere and fixed to the port plug of the integrating sphere (Thorlabs, SM05CP2C). Each sample is placed inside the integrating sphere for 3 min before taking the measurement. Measurements inside and outside the Cauchy cavity are taken for the same samples for comparison. The duration of each measurement is 5 min. The illumination power from the fiber is ~ 20 mW. To have a fair comparison, for measurements taken outside the Cauchy cavity, the source-sample distance and sample-detector distance is kept to be 2.5 cm, which is identical to the radius of the integrating sphere.

For each measurement, we were able to collect three independent parameters: the correlation function $g(\tau)$, the contrast of the correlation function β , and the count rate of the detectors. $g(\tau)$ and β are connected through the Siegert relation $g_I(\tau) = 1 + \beta g(\tau)$, where $g_I(\tau)$ represents the intensity-intensity correlation function [2]. Typically, β strongly depends on the experimental geometry. In our experiment, it represents the effect of multiple-speckle integration and two polarization states and might be used as an indicator to determine whether diffusion approximation is valid. Experimentally, β can be obtained from $\beta = g_I(\tau \rightarrow 0)$.

As mentioned before, we performed measurements at two different detection angles (45° and 135°). The results are summarized in Fig. 8. The corresponding characteristic times of the dynamics for each $g(\tau)$ are shown in Fig. 4(a). There are several observations to note here. First, due to the high reflectivity of the sphere, the measurements taken inside the cavity have higher count rates compared to outside measurements. Besides, the count rates remain unchanged when ρ changes, indicating that the technique is more robust and does not require any adjustments for a specific measurement. Also, the contrast β is constant (~ 0.48) for both cases in the diffusion regime (large ρ). One can clearly see that the Cauchy cavity has dramatically decreased (by more than one order of magnitude) the concentration limit for which the diffusion approximation can be applied. We note that the value of β is not unity mainly due to the use of nonpolarizing single-mode fibers that support two polarized modes. Finally, the measurements taken inside the cavity are not sensitive to the angle of detection, while the measurements taken outside the cavity vary greatly and in an unpredictable way when the angle of detection changes. This phenomenon is observed for all three descriptors, $g(\tau)$, β , and the count rate.

2. Retrieving particle sizes from complex systems

As a proof-of-concept experiment, we prepared samples using polystyrene particles of different diameter (from 200 nm to 3 μm) in a transparent cylindrical container, with known volume V and area Σ . The loss of the system is predetermined by calibration measurements. Therefore, the mean paths of photons $\langle s \rangle$ are calculated theoretically using Eq. (4). The l^* of these samples was adjusted to be the same by varying the concentration according to Mie calculations [29], which are 5 mm. The experimental data with corresponding fitting are shown in Fig. 9. The retrieved τ_m using Eq. (2) as well as D_m is shown in Fig. 5.

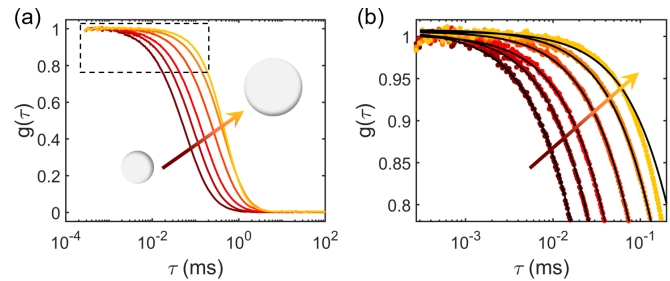


FIG. 9. (a) Experimentally measured $g(\tau)$ of different size of particles. (b) Corresponding experimental fit using single-exponential function.

- [1] B. Chu, *Laser Light Scattering: Basic Principles and Practice* (Academic Press, New York, 2007).
- [2] B. J. Berne and R. Pecora, *Dynamic Light Scattering: With Applications to Chemistry, Biology, and Physics* (Dover, New York, 2000).
- [3] D. J. Pine, D. A. Weitz, P. M. Chaikin, and E. Herbolzheimer, *Phys. Rev. Lett.* **60**, 1134 (1988).
- [4] G. Maret and P. Wolf, *Z. Phys. B: Condens. Matter* **65**, 409 (1987).
- [5] D. J. Pine, D. A. Weitz, J. Zhu, and E. Herbolzheimer, *J. Phys. (Paris)* **51**, 2101 (1990).
- [6] D. J. Durian, *Phys. Rev. E* **51**, 3350 (1995).
- [7] K. M. Yoo, F. Liu, and R. R. Alfano, *Phys. Rev. Lett.* **64**, 2647 (1990).
- [8] M. C. W. van Rossum and T. M. Nieuwenhuizen, *Rev. Mod. Phys.* **71**, 313 (1999).
- [9] I. Freund, M. Kaveh, and M. Rosenbluh, *Phys. Rev. Lett.* **60**, 1130 (1988).
- [10] R. Pierrat, P. Ambichl, S. Gigan, A. Haber, R. Carminati, and S. Rotter, *Proc. Natl. Acad. Sci. USA* **111**, 17765 (2014).
- [11] P. Dirac, British Report MS-D-5, Part I (1943).
- [12] A. Mazzolo, B. Roesslinger, and C. M. Diop, *Ann. Nucl. Energy* **30**, 1391 (2003).
- [13] S. Blanco and R. Fournier, *Europhys. Lett.* **61**, 168 (2003).
- [14] R. Savo, R. Pierrat, U. Najar, R. Carminati, S. Rotter, and S. Gigan, *Science* **358**, 765 (2017).
- [15] T. Ala-Nissila, R. Ferrando, and S. Ying, *Adv. Phys.* **51**, 949 (2002).
- [16] D. O. Riese, G. H. Wegdam, W. L. Vos, R. Sprik, D. Fenistein, J. H. H. Bongaerts, and G. Grübel, *Phys. Rev. Lett.* **85**, 5460 (2000).
- [17] A. Ishimaru, *Wave Propagation and Scattering in Random Media* (Academic Press, New York, 1978), Vol. 2.
- [18] R. Carminati, R. Elaloufi, and J.-J. Greffet, *Phys. Rev. Lett.* **92**, 213903 (2004).
- [19] M. S. Patterson, B. Chance, and B. C. Wilson, *Appl. Opt.* **28**, 2331 (1989).
- [20] J. X. Zhu, D. J. Pine, and D. A. Weitz, *Phys. Rev. A* **44**, 3948 (1991).
- [21] G. Popescu, C. Mujat, and A. Dogariu, *Phys. Rev. E* **61**, 4523 (2000).
- [22] P. Kaplan, M. H. Kao, A. Yodh, and D. J. Pine, *Appl. Opt.* **32**, 3828 (1993).
- [23] F. Martelli, D. Contini, A. Taddeucci, and G. Zaccanti, *Appl. Opt.* **36**, 4600 (1997).
- [24] L. Pattelli, R. Savo, M. Burrelli, and D. S. Wiersma, *Light: Sci. Appl.* **5**, e16090 (2016).
- [25] G. Popescu and A. Dogariu, *Opt. Lett.* **24**, 442 (1999).
- [26] G. Popescu and A. Dogariu, *Opt. Lett.* **26**, 551 (2001).
- [27] F. Tommasi, L. Fini, F. Martelli, and S. Cavalieri, *Phys. Rev. A* **102**, 043501 (2020).
- [28] O. Bénichou, M. Coppey, M. Moreau, P. Suet, and R. Voituriez, *Europhys. Lett.* **70**, 42 (2005).
- [29] C. F. Bohren and D. R. Huffman, *Absorption and Scattering of Light by Small Particles* (John Wiley & Sons, New York, 2008).
- [30] G. Batchelor, *J. Fluid Mech.* **74**, 1 (1976).
- [31] S. Blanco and R. Fournier, *Phys. Rev. Lett.* **97**, 230604 (2006).
- [32] G. Terrée, S. Blanco, M. El Hafi, R. Fournier, and J. Y. Rolland, *Europhys. Lett.* **110**, 20007 (2015).
- [33] F. Tommasi, L. Fini, F. Martelli, and S. Cavalieri, *Opt. Commun.* **458**, 124786 (2020).
- [34] V. V. Tuchin, *Tissue Optics: Light Scattering Methods and Instruments for Medical Diagnostics* (SPIE, Bellingham, WA, 2015).
- [35] C. R. Bermingham *et al.*, bioRxiv460139 (2018).
- [36] S. Kasas, F. S. Ruggeri, C. Benadiba, C. Maillard, P. Stupar, H. Tournu, G. Dietler, and G. Longo, *Proc. Natl. Acad. Sci. USA* **112**, 378 (2015).
- [37] R. G. Willaert *et al.*, *Sci. Adv.* **6**, eaba3139 (2020).
- [38] A. Caspi, R. Granek, and M. Elbaum, *Phys. Rev. Lett.* **85**, 5655 (2000).
- [39] A. G. Zilman and R. Granek, *Phys. Rev. Lett.* **77**, 4788 (1996).
- [40] A. Z. M. Badruddoza, S. V. MacWilliams, D. A. Sebben, M. Krasowska, D. Beattie, D. J. Durian, and J. K. Ferri, *Curr. Opin. Colloid Interface Sci.* **37**, 74 (2018).
- [41] X. Man and M. Doi, *Phys. Rev. Lett.* **116**, 066101 (2016).
- [42] N. Şenbil, M. Gruber, C. Zhang, M. Fuchs, and F. Scheffold, *Phys. Rev. Lett.* **122**, 108002 (2019).
- [43] J. H. Cho, R. Cerbino, and I. Bischofberger, *Phys. Rev. Lett.* **124**, 088005 (2020).
- [44] P. Hänggi and F. Marchesoni, *Rev. Mod. Phys.* **81**, 387 (2009).

- [45] J. R. Howse, R. A. L. Jones, A. J. Ryan, T. Gough, R. Vafabakhsh, and R. Golestanian, *Phys. Rev. Lett.* **99**, 048102 (2007).
- [46] R. Pastore, A. Ciarlo, G. Pesce, F. Greco, and A. Sasso, *Phys. Rev. Lett.* **126**, 158003 (2021).
- [47] H. Guo, G. Bourret, R. B. Lennox, M. Sutton, J. L. Harden, and R. L. Leheny, *Phys. Rev. Lett.* **109**, 055901 (2012).
- [48] K. M. Douglass, S. Sukhov, and A. Dogariu, *Nat. Photonics* **6**, 834 (2012).
- [49] F. Evers *et al.*, *Eur. Phys. J.: Spec. Top.* **222**, 2995 (2013).
- [50] A. Mazzolo, *Europhys. Lett.* **68**, 350 (2004).
- [51] F. Martelli, F. Tommasi, L. Fini, L. Cortese, A. Sassaroli, and S. Cavalieri, *J. Quant. Spectrosc. Radiat. Transfer* **276**, 107887 (2021).